Int. J. High Technology Ceramics **3** (1987) 43–61

High-Temperature Durability and Limits of Sintered and Hot-Pressed Silicon Nitride Materials

U. Ernstberger, G. Grathwohl and F. Thümmler

Institut für Werkstoffkunde II, Universität Karlsruhe,
Institut für Material- und Festkörperforschung,
Kernforschungszentrum Karlsruhe, Postfach 3640, D 7500 Karlsruhe 1, FRG

SUMMARY

Hot-pressed, sintered and post-sintered Si_3N_4 materials (HPSN, SSN and SRBSN, respectively) are characterized in their oxidation and creep behaviour. Commercial materials with complex microstructures including intergranular glass or partly crystallized phases are investigated. In creep and oxidation experiments a critical transition temperature, characteristic for each individual material is detected, indicating the formation of liquid phases: 1460°C for HPSN (Y), 1240°C for SSN (Y, Al and Ti) and 1300°C for SRBSN (Y, Al and Mg). The oxidation kinetics are changing considerably at these temperatures. The nature of the creep curve is transient below these temperatures, while beyond the transition temperatures rather short rupture times are measured with preceding creep stages, with minimum creep rates and accelerated creep.

1 INTRODUCTION

The application of ceramics as high-temperature materials is proposed for many purposes, e.g. in engines and energy systems. In order to replace metals for application under these severe conditions, economic production processes and outstanding properties are needed for ceramics to be considered as alternative materials to superalloys. In the high-temperature regime, the highest strength values for structural ceramics are offered by the various Si_3N_4 materials. The ZrO_2-transformation-toughened ceramics with their excellent properties at lower temperatures do not retain their microstructure and properties at temperatures above 1000°C.

Dense Si_3N_4 materials are today produced by various routes, viz. sintering, hot-pressing, post-sintering or hot-isostatic pressing. All these materials appear to be affected, if exposed to high temperatures, especially for long times in oxidizing environments. While the intrinsic properties of Si_3N_4 do not reveal any problems in the degradation of the material up to these high temperatures, the microstructures of the Si_3N_4 products for engineering purposes are characterized by residual glass phases from the liquid-phase sintering process necessary for densification. After cooling from the sintering temperature, polyphase microstructures or intergranular phases in virtually monophase Si_3N_4 microstructure are found. These intergranular films strongly influence the properties and give rise to degradation and transportation processes, which cause the behaviour of the materials to deteriorate.

It is the purpose of this work to investigate the high-temperature long-term properties of four Si_3N_4-materials from different routes. Oxidation as well as creep and creep rupture measurements were performed with two aims: to determine the high-temperature potential including critical temperature regimes and to understand the kinetics and mechanisms of the relevant microstructural processes at high temperatures.

2 MATERIALS

Four Si_3N_4 materials of commercial origin were investigated, representing different technologies and group of additives. Two hot-pressed grades (HPSN) were compared with a sintered (SSN) and a post-sintered reaction-bonded Si_3N_4 (SRBSN). The Si_3N_4 phase is in all materials present as the β- or β'-modification (see also Table 1). The HPSN materials make essentially use of a single oxide (MgO or Y_2O_3) as sintering additive, i.e. HPSN (Mg) and HPSN (Y), while in the pressureless sintered materials a combination of oxides is added to improve densification: SSN (Y, Al and Ti) and SRBSN (Y, Al and Mg). The compositions of the sintered products as determined by chemical analysis are listed in Table 2.

TABLE 1
Major Phases Present in the Microstructure of the Investigated Si_3N_4 Materials

Material	*Type of additive*	*Phases present*
HPSN (Mg)	MgO	β-Si_3N_4, glass
HPSN (Y)	Y_2O_3	β-Si_3N_4, $Y_5(SiO_4)_3N$, glass
SSN (Y, Al, Ti)	Y_2O_3, Al_2O_3, TiO_2	β'-Si_3N_4, $Y_2Si_2O_7$, glass
SRBSN (Y, Al, Mg)	Y_2O_3, Al_2O_3, MgO	β'-Si_3N_4, $Si_3N_4 \cdot Y_2O_3$, glass

TABLE 2
Chemical Analysis of the Investigated Silicon Nitride Materials[a]

	HPSN (Mg)	*HPSN (Y)*	*SSN (Y, Al, Ti)*	*SRBSN (Y, Al, Mg)*
Y	n.d.[b]	4·63	3·61	3·5
Mg	1·77	0·03	0·014 5	0·25
Al	0·407	0·12	2·6	0·545
Ti	n.d.	n.d.	0·67	0·055
Fe	1·43	1·77	0·055	0·295
Ca	0·10	0·02	0·035	0·06
O	2·0	2·1	4·305	1·9
N	37·1	35·9	35·15	36·85
C	0·713	0·297	0·705	0·17
W	n.d.	n.d.	<0·05	<0·05
Mn	n.d.	n.d.	<0·02	<0·02
Cr	n.d.	n.d.	<0·01	0·06
Ni	n.d.	n.d.	n.d.	n.d.
Li	<0·005	0·02	n.d.	n.d.

[a] Measured as wt%.
[b] n.d. = not determined.

All investigated materials were of high density, i.e. between 3·2 and 3·3 $Mg\,m^{-3}$. While the HPSN samples reach densities of nearly 100% theoretical density, the sintered products end up with values of 98·5% (SRBSN) and 99·2% (SSN). The microstructures of these Si_3N_4 materials are characterized by very fine β-Si_3N_4 grains, which contain some amounts of Al and O in solid solution in the case of SSN and SRBSN. In Fig. 1, TEM micrographs are presented for all four materials. In contrast to the other three, HPSN (Mg) shows only few elongated grains and rather rounded grain shapes and edges. As also investigated by using TEM, a wide distribution of the grain sizes is observed in all products with few larger grains up to some μm in length (e.g. 10 μm) and with many small globular grains below 1 μm. The smallest average grain size is found in the SSN-product.

By X-ray diffraction analysis the existence of the main crystalline phases could be ascertained. Besides β- and β'-Si_3N_4, respectively, traces of various Y–Si–O–N phases and impurities were detected as listed in Table 1.

The microstructures of all these materials contain intergranular glass phases. In the case of HPSN (Y) and SRBSN the intergranular phase is partly crystalline, while it is completely amorphous in SSN in the as-delivered state. An example for the latter material is given in Figs 2(a) and 2(b) where the amorphous phase is shown to be extended from a two-grain

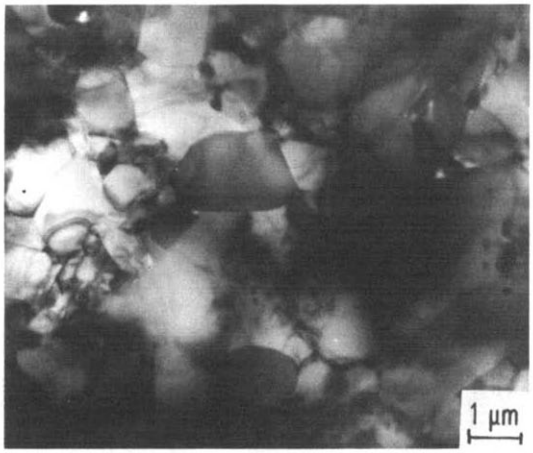

(a)

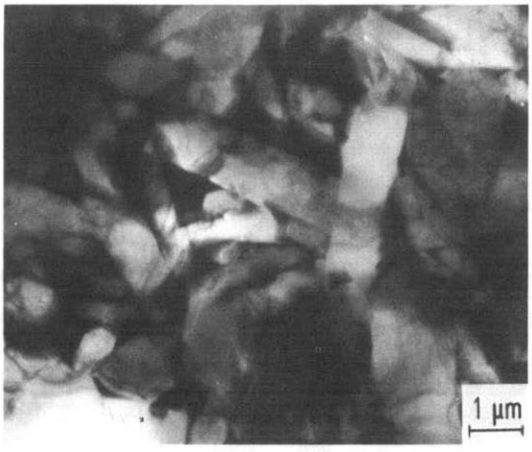

(b)

Fig. 1. TEM micrographs of the four Si_3N_4 materials: (a) HPSN (Mg); (b) HPSN (Y); (c) SSN; (d) SRBSN.

channel into a triangular pocket. An annealing procedure at 1200°C (200–1000 h in air) was applied to SSN in order to reach partial crystallization of this phase (Figs 2(c) and (d)). Crystallization was essentially limited to the larger pockets in the three- or four-grain junctions; the thin films do not crystallize during this treatment. Thus, the thin amorphous films (1–5 nm) of the intergranular phase are to be taken as important microstructural features of all investigated materials.

The analysis of the intergranular phases in these commercial products has not yet led to a final and comprehensive statement. Besides the role of the

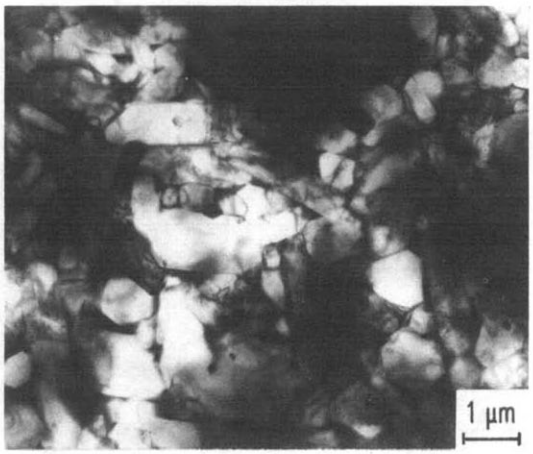

(c)

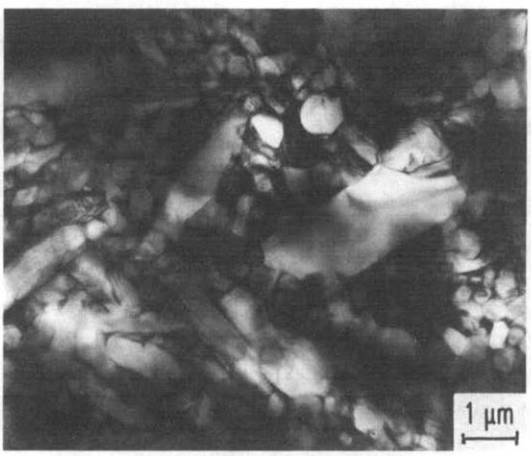

(d)

Fig. 1.—*contd.*

intentional constituents the effect of the impurities has to be noted, since the common impurity elements (e.g. Ca, Na and Fe) are readily accommodated in the intergranular phases.[1] In Fig. 3, some representative results of the composition of intergranular phases are illustrated, as measured by STEM–X-ray energy-dispersive spectroscopy.[2] In HPSN (Mg) (Fig. 3(a)), the intergranular phase forms a glass with a Mg/Si ratio close to the eutectic value (SiO_2–$MgSiO_3$). However, phase separation and formation of Si_2N_2O and $MgSiO_3$ crystallites seem also to be possible,[3] although not detectable in our study. In HPSN (Y), a crystalline Y-Si-oxinitride is observed between the

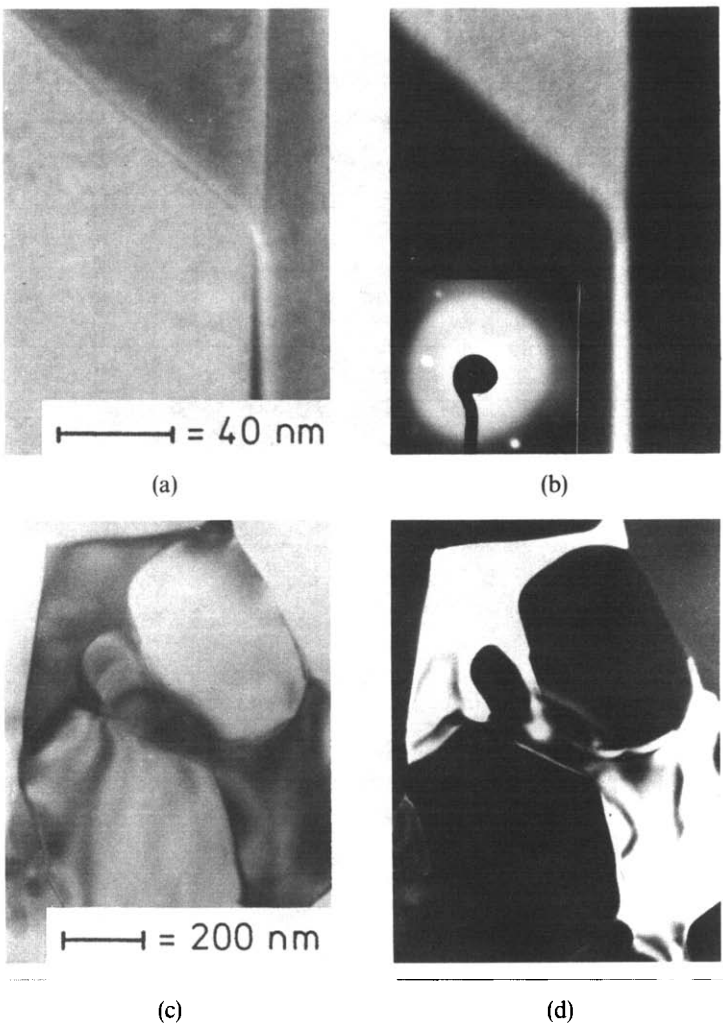

Fig. 2. Bright field (a, c) and dark field (b, d) transmission micrographs showing the intergranular phase in the as-delivered state (a, b) and after heat treatment (1200°C, 1000 h in air) (c, d) of SSN.

β-Si_3N_4 phase, both being separated by a 2–3 nm thick glass phase. The intergranular phases in the sintered materials are rather inhomogeneous in their concentrations. In general, very different concentration ratios were measured on different spots in one sample. Results are also given for SSN and SRBSN in Figs 3(c) and 3(d), respectively.

The materials contain generally two types of inclusions. Intergranular inclusions with sizes similar to the Si_3N_4 grains are observed besides much smaller intergranular inclusions (0·03–0·7 μm). For both types, examples are shown in Fig. 4. A relatively high number of intragranular Si–Ti inclusions

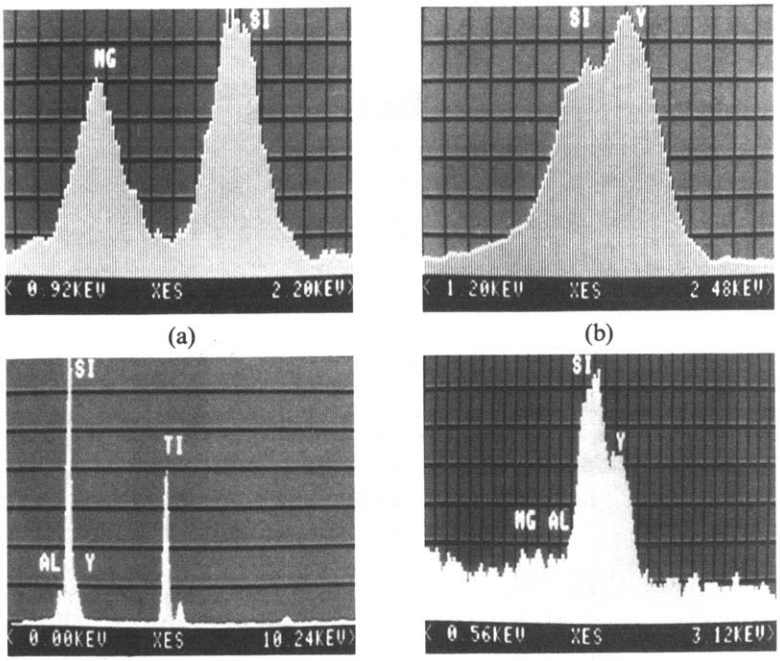

Fig. 3. Analysis of intergranular phases (triple points) in Si_3N_4 materials by STEM X-ray energy-dispersive spectroscopy (EDS): (a) HPSN (Mg); (b) HPSN (Y); (c) SSN; (d) SRBSN.

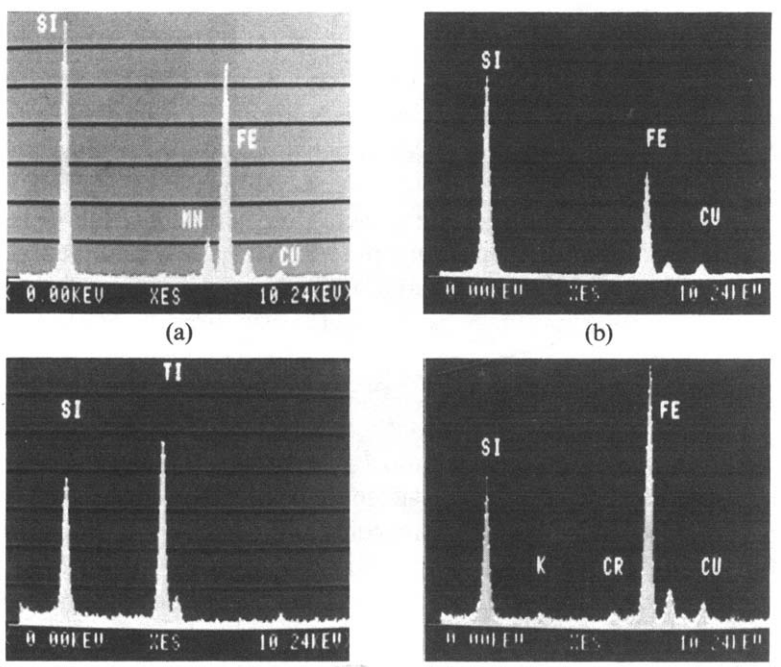

Fig. 4. STEM–X-ray EDS results of inclusions of Si_3N_4 materials: (a) HPSN (Mg), intergranular; (b) HPSN (Y), intergranular; (c) SSN, intragranular; (d) SRBSN, intergranular.

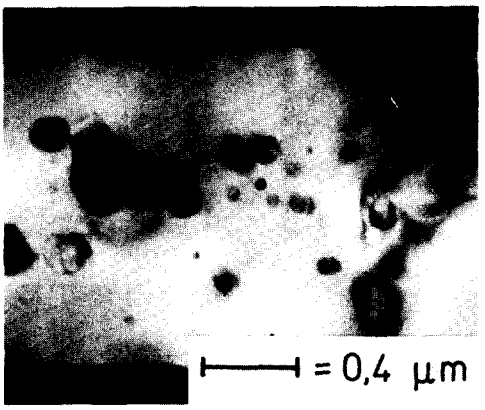

Fig. 5. Intragranular inclusions in a Si_3N_4 grain in SSN.

are found in SSN (Fig. 4(c)), while in the other materials intergranular Si–Fe inclusions predominate (Figs 4(a), (b) and (d)). The morphology and distribution of the intragranular inclusions in SSN are manifested in Fig. 5.

3 EXPERIMENTAL PROCEDURE

The experiments to study oxidation and creep were both performed using bars with the cross-section 3·5 × 4·5 mm. For the creep tests the bending bars were 45 mm long, and for oxidation tests about 22 mm. The oxidation kinetics were studied in a thermogravimetric device using dry air under normal pressure at test temperatures between 1000 and 1500°C. The surfaces of the oxidation and creep specimens were polished before the tests. In all oxidation experiments the conditions necessary to allow passive oxidation to take place[4] were fulfilled. Thus, the oxidation reaction was followed by measuring the isothermal mass gain $\Delta m/A$ versus time t, according to the general equation

$$(\Delta m/A)^n = k_p \cdot t \tag{1}$$

with A = specimen surface and n and k_p being constants.

Creep was measured using a four-point bending fixture with the distances for the outer and inner loading points being 40 and 20 mm, respectively. The tests were performed in air at temperatures between 1100 and 1480°C. All components of the equipment being in contact with the specimen and the heating elements were made from SiC. Constant load tests were continued up to the rupture of the specimen or to about 200 h. The specimen deformation was measured continuously as midpoint deflection on the tension surface of the bending bar. Linear variable differential transducers

with a sensitivity of about 0·1 mm V^{-1} were used. Stress and strain were calculated using elastic beam equations.[5]

4 RESULTS

4.1 Oxidation

The results of the oxidation tests as measured in the thermogravimetric system over 72 h are presented in Fig. 6 as isothermal mass gain curves in $\log \Delta m/A$ vs. $\log t$ plots. With $n = 2$, as noted in Fig. 6, an oxidation proceeds according to a parabolic law (eqn 1). From Fig. 6 it first becomes evident that, in a temperature region where true parabolic oxidation behaviour is observed, HPSN (Mg) exhibits the highest k_p values compared with all other materials (see also Fig. 7). The oxidation follows the parabolic law over the whole test duration up to 1200°C. At higher temperatures and longer times, deviation to lower rates is observed. In contrast, the oxidation behaviour of HPSN (Y) is best described after the first few hours by a logarithmic law. The oxidation curves (Fig. 6(b)) are close together; the excellent oxidation resistance of this material goes along with a rather small influence of temperature on the oxidation rates. The oxidation resistance is lowered only at temperatures above 1450°C where oxidation proceeds in a way similar to the parabolic law.

The sintered materials exhibit a more complex oxidation behaviour. For SSN, parabolic kinetics are observed at the lower ($\leq$1200°C) and the highest (1500°C) temperatures, but not at the intermediate temperatures. A temperature level around 1240°C is noted, where the oxidation kinetics change discontinuously and the rates increase sharply. A similar behaviour is observed with SRBSN, with the characteristic difference that the parabolic oxidation range at the lower temperatures is extended up to about 1320°C.

In Fig. 7 the oxidation results are collected in an Arrhenius diagram of the parabolic rate constants k_p. The highest k_p values for the investigated materials are revealed by HPSN (Mg) at all temperatures. An apparent activation energy of about 500 kJ mol^{-1} can be calculated over the whole temperature range. Much smaller temperature increments were measured for HPSN (Y), but the values cannot really be compared due to the fact that the curves are not truly parabolic. However, these data may be compared with results from other authors,[6] illustrating the fact that at a temperature around 1460°C a change in the oxidation mechanism occurs. A strong variation in the activation energies is measured for the sintered materials with very low values of about 100 kJ mol^{-1} at the lower temperatures ($\leq$1100°C), which is similar to the value for HPSN (Y) at all temperatures up

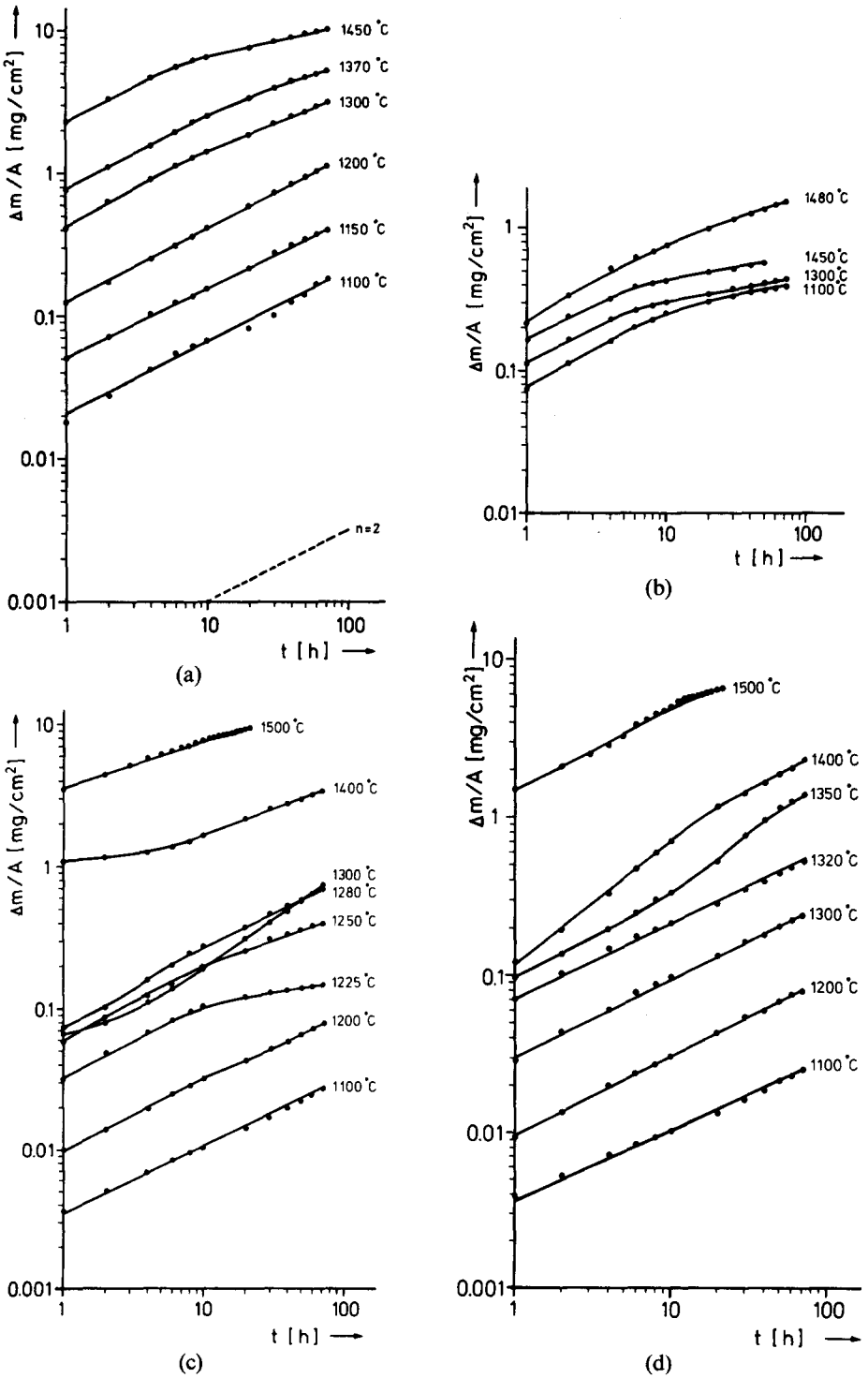

Fig. 6. Isothermal oxidation curves of four Si_3N_4 materials in dry air: (a) HPSN (Mg); (b) HPSN (Y); (c) SSN; (d) SRBSN.

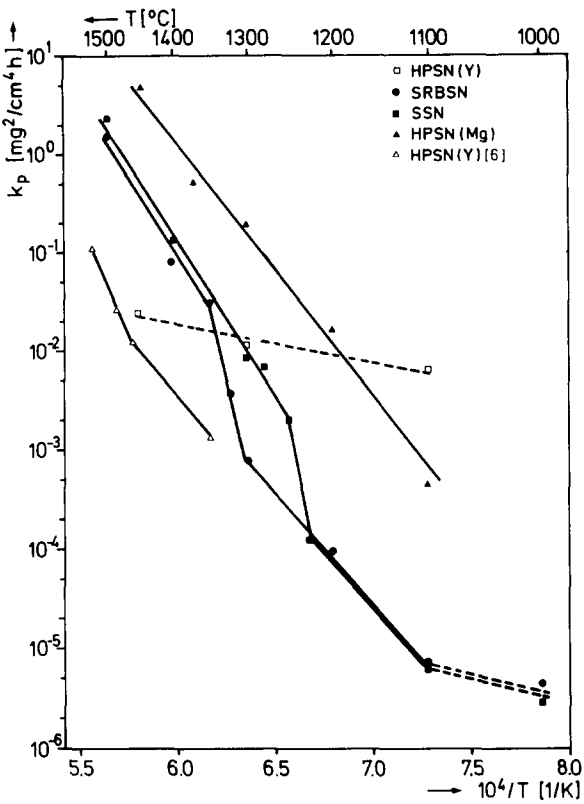

Fig. 7. Arrhenius diagram of the parabolic oxidation rate constant of several Si_3N_4 materials.

to 1460°C. The sintered materials reveal at higher temperatures (> 1100°C) an increased temperature dependence of the rate constant leading to an activation energy of about 420 kJ mol^{-1}. This value is valid up to 1240 and 1320°C for SSN and SRBSN, respectively, where the rates change discontinuously and the calculation of an activation energy is not meaningful. Above these temperature ranges the oxidation of the sintered materials is to be described by high activation energies of about 620 kJ mol^{-1}.

4.2 Creep

The creep curves are presented in Fig. 8 in the form of $\log \dot{\varepsilon}$ vs. $\log t$ plots. This type of diagram was chosen, since the creep behaviour is of transient nature over a wide range of loading parameters. All materials start in the experiment with relatively high creep rates ($\dot{\varepsilon}$), which then continue to decrease over very long times (e.g. > 100 h), mainly at lower temperatures.

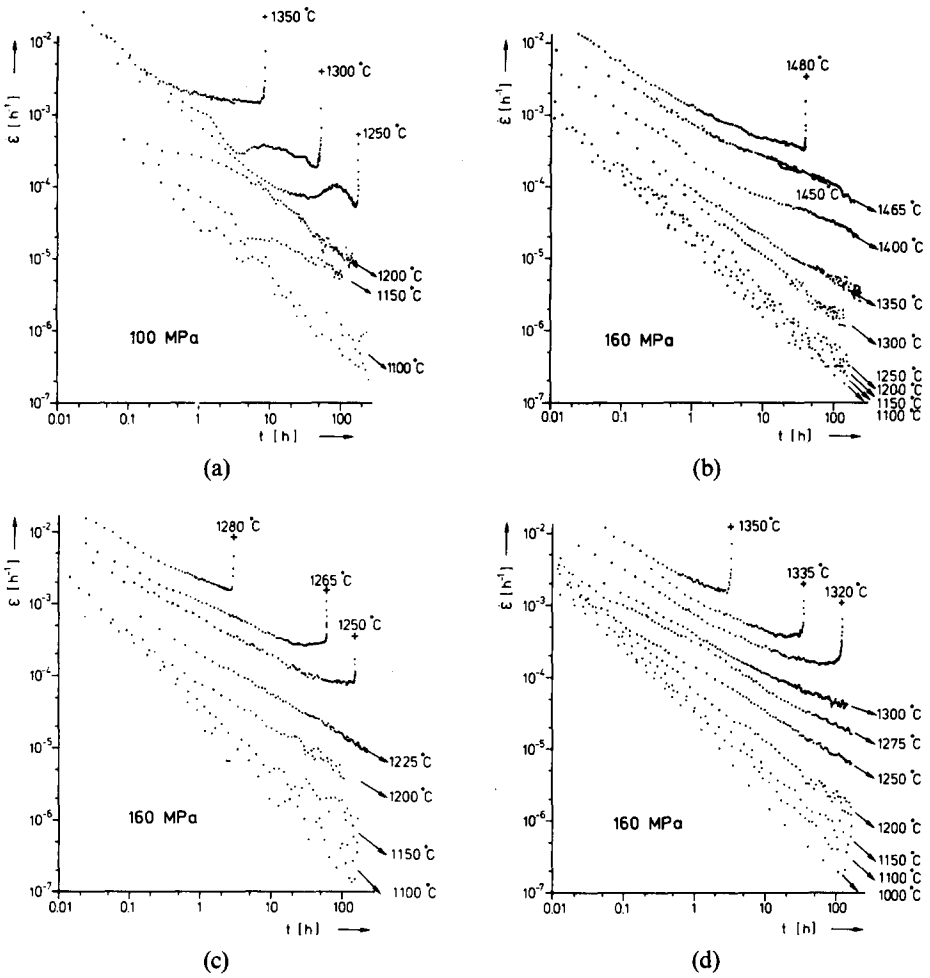

Fig. 8. Creep curves of four Si_3N_4 materials in air at different temperatures: (a) HPSN (Mg); (b) HPSN (Y); (c) SSN; (d) SRBSN.

The creep rate can then be reduced by more than 3 orders of magnitude. This behaviour can be described by the relation $\dot{\varepsilon} = at^{-c}$, with a factor a and the time exponent c. In making use of this relation it becomes clear from the results in Fig. 8, that at rather low temperatures (e.g. 1100°C) c values near 1 are measured. This corresponds with a logarithmic creep law.

With increasing temperatures the slopes of the creep curves get less steep, and the time exponent c is gradually lowered and reaches a minimal value around 0·5 at a temperature T_t, which is characteristic for each individual material. This temperature is determined by the experiments as 1470, 1240 and 1300°C for HPSN (Y), SSN and SRBSN, respectively. These values can be compared with the critical temperatures for oxidation discussed before.

It may be noticed that, under the conditions of these experiments, the primary creep ends in the stage of secondary creep and leads then to tertiary creep and creep rupture only at temperatures as high as T_t or higher. Below T_t these materials can retain their increasing creep resistance over very long periods. However, the creep increases strongly in a very small temperature interval around T_t, e.g. between 1225 and 1250°C for SSN.

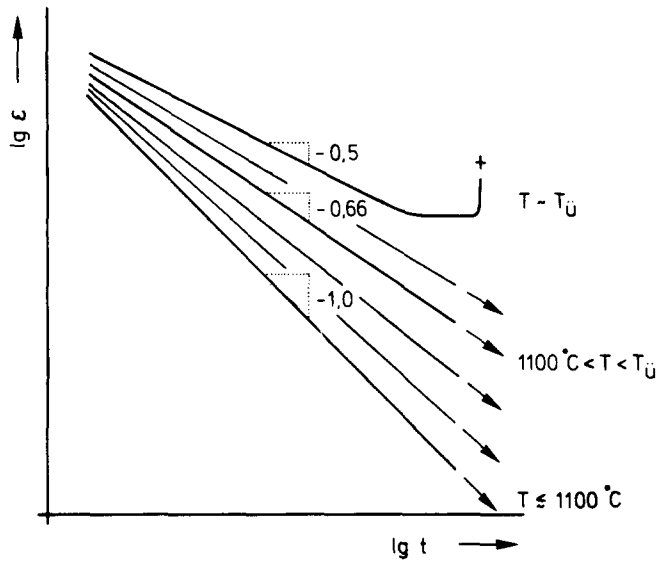

Fig. 9. Schematic diagram of the time and temperature dependencies of the creep rate.

These results are collected in Figs 9 and 10. Figure 9 typifies the creep kinetics at different temperatures. Starting from a pure transient creep behaviour with $c = 1$ at the lower temperatures, a decreasing c value is observed with increasing temperature. It is only at a value of $c = 0{\cdot}5$, where the transition of primary to secondary creep seems to be possible. However, an extended steady-state creep stage is not observed. Secondary creep is always followed by tertiary creep and creep rupture, after relatively small portions of strain generated in the secondary stage. It is then conjectured that this secondary creep reflects in fact a superposition of the primary creep with tertiary creep elements.

In Fig. 10 the time exponent c is shown as a function of temperature for three materials. This temperature dependence is rather similar for the different materials, but on different temperature levels. The value $c = 0{\cdot}5$, measured at T_t, can be used to characterize the materials and the different weakening behaviour of their intergranular phases. The creep curves of HPSN (Mg) are not to be typified in the same way. It is suggested that creep is

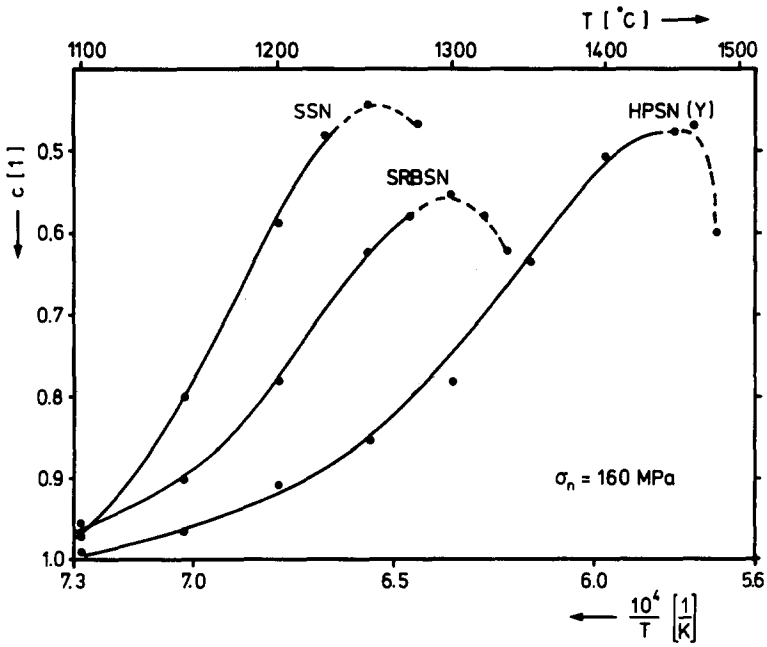

Fig. 10. Temperature effect on the time exponent c of the transient creep equation.

affected by more than just one mechanism, which leads to a more complicated creep curve with alternating creep rates, superimposed on an overall primary creep behaviour (Fig. 8(a)).

5 DISCUSSION

The kinetics and the mechanisms controlling the oxidation behaviour of Si_3N_4 materials depend on the type of additives used for densification. HPSN (Mg) with the highest oxidation rate constants (see Fig. 7) forms an oxide scale which is not protecting against further oxidation. This is proved by reoxidation experiments[2,6] (oxidation after removing the oxide surface scale generated in the first part of the test). Since the oxidation curve proceeds, after removing the original oxide scale, continuously into the second part it can be concluded that the diffusion-controlled oxidation of HPSN (Mg) is not dependent on a process in the oxide scale. The outward diffusion of Mg in the intergranular phase contributing to a high Mg-containing oxide scale and leading to a gradient of the Mg concentration in the bulk may control the oxidation rate.[2,7] Examples of these gradients are shown in Fig. 11 as measured by wavelength-dispersive X-ray microanalysis. The formation of the Mg gradient can also explain the fact that the

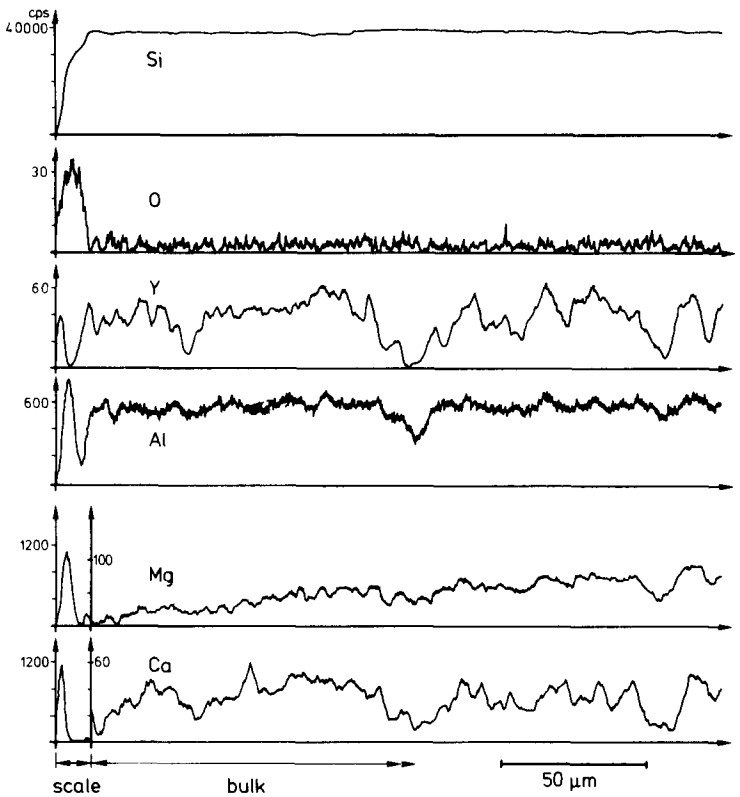

Fig. 11. Concentration profiles in an oxidized SRBSN material (1300°C, 72 h, in air) as measured by wavelength-dispersive X-ray microanalysis.

oxidation rate slows down, at high temperatures after longer times, when the sample is depleted in its Mg content below the oxide scale (Figs 6(a) and (d)).

All other materials are controlled in their oxidation behaviour by diffusion processes in the scale. By re-oxidation experiments it became clear that the oxide scale has a protective effect on all other samples. A concentration gradient in the bulk material was only measured for Mg, but not for the other sintering additives (Fig. 11). Thus, the O_2 diffusion in the SiO_2 layer is suggested to be rate controlling as far as no microcracking prevents the protecting effect of the scale. The temperature dependence of the rate constant is interrupted at about 1240 and 1310°C for SSN and SRBSN, respectively, by a discontinuity that is supposed to be caused by the occurrence of first liquid phases.

The same transition temperatures, T_t, are found to play a critical role in the creep behaviour of these materials. Below these critical temperatures creep is of transient nature under all conditions realized in this study. This is manifested in additional creep curves (Fig. 12) where the stress effect on

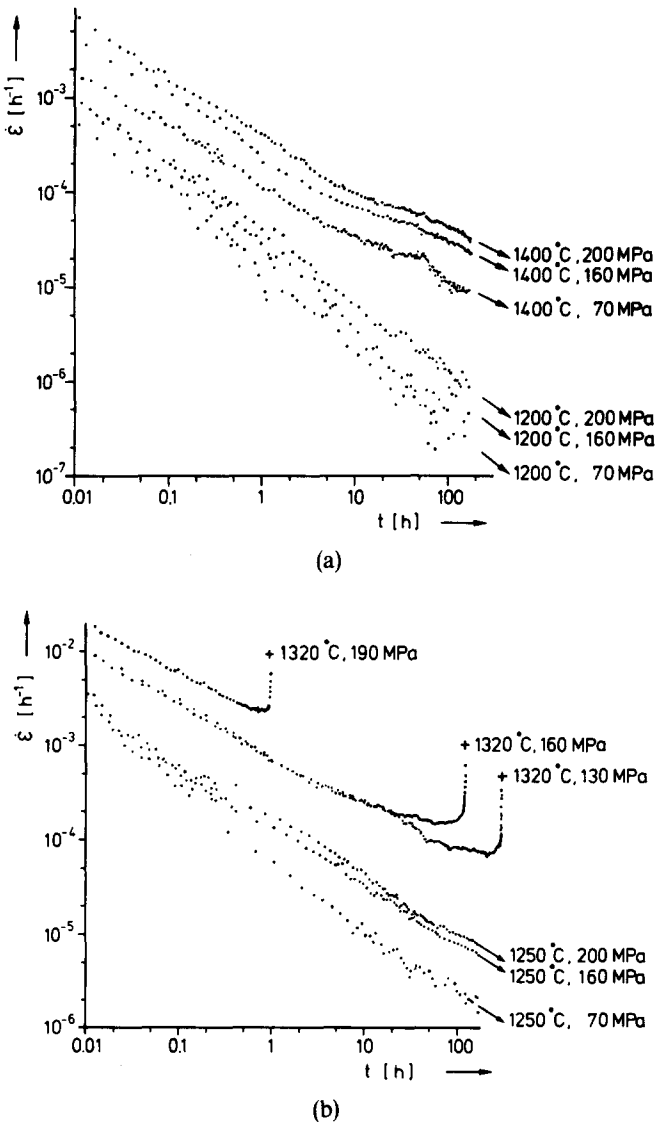

Fig. 12. Stress dependence of the creep curves at various temperatures: (a) HPSN (Y); (b) SRBSN.

creep is investigated. As long as the test temperature is not higher than the critical temperatures T_t (Figs 12(a) and 12(b), 1250°C), creep is characterized by its transient nature over the total test duration (*ca.* 200 h) and the range of stresses used in these tests (≤ 200 MPa). No failure was observed under these conditions and the specimens hardly showed any sign of cavitation. After longer times or at higher stresses than used in this study the specimens may break due to the phenomenon of slow crack growth.

In Fig. 12(b) it is shown what dramatic influence of the test temperature is possible by surpassing the critical temperature T_t. At $T > T_t$, which is the case at 1320°C for SRBSN, the creep resistance is determined by the appearance of liquid intergranular phases; thus, the conditions for heavy cavitation and creep damage are fulfilled in our tests. It becomes evident from Fig. 12(b) that the pure transient creep character is then abandoned. Rather early failure is observed, which follows a preceding tertiary creep range and an intermediate stage with a minimum in the creep rate. It becomes clear that a calculation of the stress dependence of this minimum creep rate is meaningless. These creep curves are already controlled by processes leading to rupture and the minimum creep rates do not represent true steady-state creep mechanisms. It is supposed that the minimum creep rates manifest the result of overlapping tertiary and primary creep components. It is therefore important to measure the creep curves completely in order to understand the creep kinetics correctly.[8]

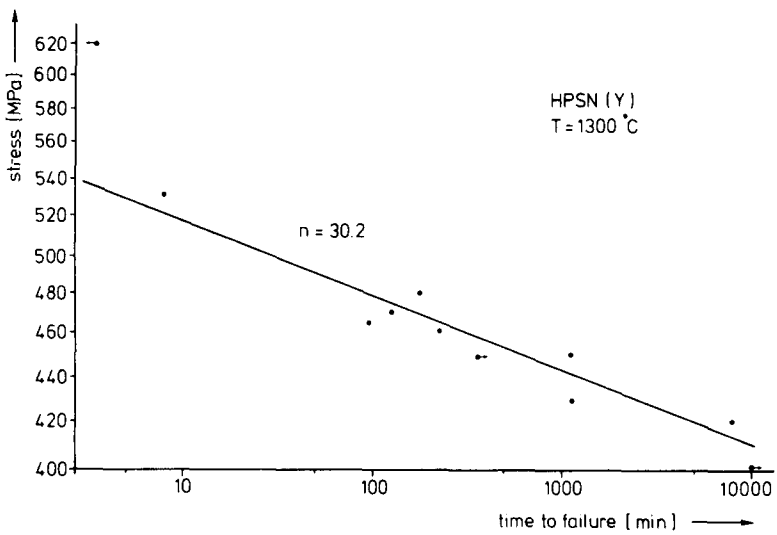

Fig. 13. Stress rupture diagram of HPSN (Y) at 1300°C.

The same is true for the interpretation of the creep rupture events. As shown in Fig. 13 for HPSN (Y) the stress–time to failure relationship under constant load conditions can be measured in similar test periods as used for the creep tests if the stress is increased beyond 400 MPa. Since the test temperature (1300°C) is below T_t for HPSN (Y) and the creep deformation is not too large,* the stress–time to failure relationship may be interpreted in a simplified manner on the basis of the equation for slow crack growth rate,

* The stress sensitivity of the transient creep curves is not very pronounced (see Fig. 12).

$v \sim K_I^n$.[9] The exponent n of the stress intensity factor K_I is then often used to characterise the slow crack growth behaviour. Using the conventional approximations a value of 30·2 is determined for HPSN (Y) by the tests at 1300°C presented in Fig. 13.

This treatment is definitely not appropriate any more under conditions of true creep rupture as discussed before.[10] Presumably at temperatures above T_t where heavy cavitation is observed during creep, the conditions for a new strain-controlled rupture criterion becomes valid for a range of lower stresses. With the phenomenon of crack blunting,[11] creep damage can be generated in a distribution all over the specimen volume. Rupture would then occur not according to slow crack growth relations, but after a critical creep strain is reached. This would be measured with HPSN (Y) only above 1480°C, but also under rather low stresses.

6 CONCLUSIONS

Dense silicon nitride materials of commercial origin were investigated, measuring their high-temperature oxidation, creep and creep rupture. The essential features of the complex microstructures are the β- or β'-phase, various intergranular crystalline phases and a glass film of 1 to 5 nm thickness between the grains in all materials.

A parallelism in the temperature dependence of creep and oxidation was detected and a characteristic temperature T_t for each individual material was determined, being decisive for the materials performance. At this transition temperature T_t the first occurrence of liquid phases in the microstructure is indicated, which leads to serious effects on the properties. These temperatures were measured as 1460°C for HPSN (Y), 1240°C for SSN and 1300°C for SRBSN.

Oxidation of HPSN (Mg) may be controlled by Mg diffusion in the intergranular phase, forming a Mg-rich scale. For the other materials the oxidation scale has a protective character, i.e. diffusion in the oxide layer controls oxidation kinetics, under the conditions used in this study. Thus, the oxidation rate increases sharply when the transition temperature is reached.

Creep is of transient nature as long as test temperatures below T_t are concerned. While at the lower temperatures ($\leq$1100°C) a pure logarithmic creep is observed, the time exponent of the transient creep equation gradually arises with increasing temperature. At the transition temperatures the creep rate follows the $t^{-0.5}$ law. Simultaneously, creep is then extended into a secondary creep stage, which represents a minimum in the creep rate rather than a true steady-state creep mechanism. This minimum creep rate is followed by tertiary creep and creep rupture.

Rupture is controlled by slow crack growth at temperatures below T_t; at higher temperatures creep of these polyphase materials is always accompanied by damaging processes, e.g. cavitation and microcracking. While at a high stress level, rupture is again controlled by the subcritical growth rate of the dominating crack, creep rupture under low stresses is reached and controlled by a critical creep strain.

REFERENCES

1. Clarke, D. R., The microstructure of nitrogen ceramics, in *Progress in Nitrogen Ceramics*, Ed. F. L. Riley, Martinus Nijhoff Publ., Boston, 1983, 341–58.
2. Ernstberger, U., *Oxidation and Creep Behaviour of Dense Silicon Nitride Materials with Different Compositions*, Diss. Universität Karlsruhe, KfK 3966, 1985.
3. Clarke, D. R., Zaluzec, N. J. and Carpenter, R. W., The intergranular phase in hot-pressed silicon nitride: II. Evidence for phase separation and crystallization, *J. Am. Ceram. Soc.*, **64** (1981) 608–11.
4. Wagner, C., Passivity during the oxidation of silicon at elevated temperatures, *J. Appl. Phys.*, **29** (1958) 1295–7.
5. Ilschner, B., *Hochtemperaturplastizität*, Springer-Verlag, Berlin, 1973.
6. Cubiciotti, D. and Lau, K. H., Kinetics of oxidation of yttria hot-pressed silicon nitride. *J. Electrochem. Soc.*, **126** (1978) 1723–8.
7. (a) Clarke, D. R. and Lange, F. F., Oxidation of Si_3N_4-alloys: relation of phase equilibria in the system Si_3N_4–SiO_2–MgO, *J. Am. Ceram. Soc.*, **63** (1980) 585–93; (b) Clarke, D. R., Thermodynamic mechanism for cation diffusion through an intergranular phase: application to environmental reactions with nitrogen ceramics, in *Progress in Nitrogen Ceramics*, Ed. F. L. Riley, Martinus Nijhoff Publ., Boston, 1983, 421–6.
8. Grathwohl, G., Creep and fracture of hot-pressed silicon nitride with natural and artificial flaws, in *Creep and Fracture of Engineering Materials and Structures*, Eds B. Wilshire and D. R. J. Owen, Pineridge Press, Swansea, 1984, 565–77.
9. Wiederhorn, S. M. and Fuller, E. R. Jr., Structural reliability of ceramic materials, *Mater. Sci. Eng.*, **71** (1985) 169–86.
10. Grathwohl, G., Regimes of creep and slow crack growth in high-temperature rupture of hot-pressed silicon nitride, in *Deformation of Ceramics II*, Eds R. E. Tressler and R. C. Bradt, Plenum Press, New York, 1984, 573–86.
11. Dalgleish, B. J., Slamovich, E. B. and Evans, A. G., Duality in the creep rupture of a polycrystalline alumina, *J. Am. Ceram. Soc.*, **68** (1985) 575–81.

Received 14 July 1986; revised version received 12 January 1987; accepted 29 January 1987